Electron-Beam Mapping of Vibrational Modes with Nanometer Spatial Resolution

C. Dwyer,[1,*] T. Aoki,[2] P. Rez,[1] S. L. Y. Chang,[2] T. C. Lovejoy,[3] and O. L. Krivanek[3,1]
[1]Department of Physics, Arizona State University, Tempe, Arizona 85287, USA
[2]LeRoy Eyring Center for Solid State Science, Arizona State University, Tempe, Arizona 85287, USA
[3]Nion Company, 11511 NE 118th Street, Kirkland, Washington 98034, USA
(Received 1 June 2016; published 15 December 2016)

We demonstrate that a focused beam of high-energy electrons can be used to map the vibrational modes of a material with a spatial resolution of the order of one nanometer. Our demonstration is performed on boron nitride, a polar dielectric which gives rise to both localized and delocalized electron-vibrational scattering, either of which can be selected in our off-axial experimental geometry. Our experimental results are well supported by our calculations, and should reconcile current controversy regarding the spatial resolution achievable in vibrational mapping with focused electron beams.

DOI: 10.1103/PhysRevLett.117.256101

Introduction.—It has recently become possible to use high-energy electrons in a scanning transmission electron microscope (STEM) to perform vibrational spectroscopy of materials [1–3]. While more-established vibrational-spectroscopic techniques, such as Raman scattering and infrared absorption, are applicable primarily to samples having at least micrometer dimensions, a highly focused electron beam should allow mapping of the vibrational spectra of materials at nanometer, or even subnanometer, spatial resolution. Such spatial resolutions have been demonstrated for substrate sample geometries using tip-enhanced Raman scattering in scanning tunnelling microscopy [4,5]. Vibrational spectroscopy in the STEM, on the other hand, would enable nanometer-scale mapping of vibrational modes, e.g., due to interfaces or defects, in a broad class of freestanding materials, free of thick substrates.

However, recent analyses of the scattering physics of electron-induced vibrational excitations [6–12] have reached contradictory conclusions about the attainable spatial resolution. Some of them have claimed that sub-nm, and even atomic, spatial resolution should be achievable [6,8], while others have stressed that, in practice, the spatial resolution will remain limited by the long-ranged electron-dipole interactions [7]. Thus far, the STEM experiments have supported the latter view, achieving spatial resolutions of only several tens of nm at best, a far cry from the sub-nm resolution routinely achieved in other forms of high-energy electron-beam imaging and spectroscopy.

Here, we demonstrate better than 2 nm spatial resolution in vibrational spectroscopy using a focused electron beam, advancing current state-of-the-art STEM results [1–3] by at least 1 order of magnitude, and several orders of magnitude better than that permitted with the more-established vibrational spectroscopies. We achieve this using an off-axial beam geometry that isolates the localized vibrational scattering from the delocalized dipole scattering, hence vastly improving the spatial resolution, extending it into the one-nanometer regime. Good quantitative agreement between our experimental results and our electron scattering calculations strongly supports our conclusions. Our results open the door to nanometer-scale electron-beam mapping of vibrational modes as a powerful tool for nanomaterials analysis.

Dipole vs localized vibrational scattering.—For our demonstration, we use hexagonal boron nitride, a polar dielectric exhibiting mixed covalent-ionic bonding. The vibrational properties of *h*-BN make it very well suited to the present study of spatial resolution. A first-principles calculation [13] of the material's vibrational (phonon) mode energies is shown in Fig. 1. These calculations agree with recent experimental data [18] and other calculations in the literature [19,20]. The four highest-energy optical modes are of particular interest here. These are modes in

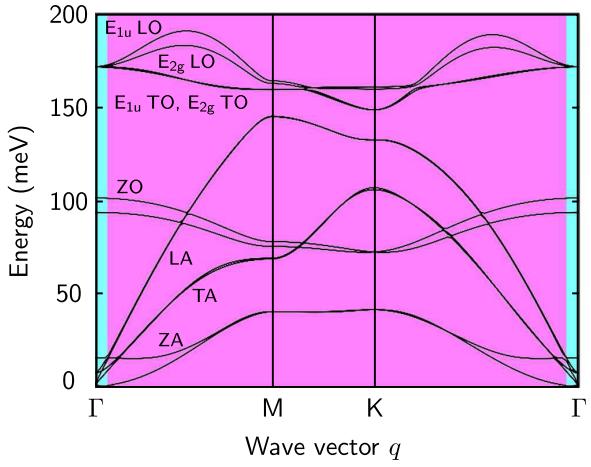

FIG. 1. Density-functional-theory calculation of *h*-BN's vibrational (phonon) energies for major symmetry paths in the Brillioun zone basal plane. Long-wavelength (cyan) and shorter-wavelength vibrations (magenta) are indicated.

 © 2016 American Physical Society

which the boron (cation) and nitrogen (anion) atoms vibrate within the (0002) atomic planes in antiphase.

In bulk samples, long-wavelength E_{1u} LO modes give rise to macroscopic depolarizing fields, causing their energy near the Γ point to increase by about 30 meV (LO-TO splitting). In our experiments, the observed energy increase is smaller (5–10 meV), due to sample size and shape effects reducing the depolarization field (our sample geometry is described below). Hence the LO-TO splitting has been omitted in Fig. 1 to better represent our experiments. Nonetheless, in finite samples, modes analogous to the long-wavelength E_{1u} LO modes produce long-ranged electric fields both inside and outside the sample. Hence, such modes can be excited by beam electrons passing at relatively large distances, up to the so-called "delocalization distance" v/ω permitted by the inelastic scattering physics, where v is the beam electron's velocity and $\hbar\omega$ is the vibrational excitation energy. For the E_{1u} LO modes in BN, $v/\omega \approx 500$ nm, and indeed we detect the excitation of these modes—the dipole scattering—even when our electron beam is made to pass hundreds of nm outside the sample (see below). (A detailed study of this effect is made in Ref. [21].) Such long-wavelength excitations necessarily involve small momentum transfers and scattering angles, the latter being of the order of μrad. Moreover, the delocalized nature of the dipole scattering implies a comparatively large scattering cross section. The dominance of dipole scattering in the STEM experiments thus far has precluded vibrational mapping with high spatial resolution.

Larger wave vectors, on the other hand, involve rapidly modulated cation-anion displacements, for which long-ranged electric fields are absent. Such modes can only be excited by beam electrons passing in the immediate vicinity of an atomic ion—the localized scattering—facilitating higher spatial resolution. Crucially, localized scattering involves larger momentum transfers and scattering angles. In this work, the key has been to configure the geometry such that the low-angle dipole scattering can be separated from the higher-angle localized scattering.

Experimental.—We use an UltraSTEM 100 (Nion Co.) to form a highly focused beam of 60 keV electrons which is scanned across an electron-transparent sample. Electron energy-loss spectroscopy (EELS) is performed as the beam is scanned. The beam position is monitored using a signal acquired simultaneously by an annular dark-field (ADF) detector. Aberration-corrected optics are capable of focusing the beam to a crossover 0.1 nm in diameter. Here, however, for reasons that will become apparent, we employ a larger probe size of the order of 1 nm. A monochromator is a special feature of our instrument [22], permitting an energy resolution of better than 20 meV in EELS.

Figure 2 shows our beam geometry. Electrons are scattered by the crystalline sample both elastically and inelastically. Figure 2(a) depicts two "elastic beams," labeled "0" (forward-scattered beam) and "g" (crystal-diffracted beam). Whereas a conventional setup for spatially resolved EELS uses an axially aligned beam, we have purposefully applied a tilting deflection before the sample, which translates the diffraction pattern relative to the EELS collection aperture. Tilting the beam, rather than moving the collection aperture, avoids the introduction of post-objective aberrations detrimental to the energy resolution. The incidence angle α is chosen such that the elastic beams do not overlap. In the regions of the diffraction pattern occupied by elastic beams, the vibrational scattering is dominated by low-angle dipole scattering (because of its larger cross section). Between the elastic beams, the vibrational scattering is necessarily higher-angle and localized. The beam tilt controls

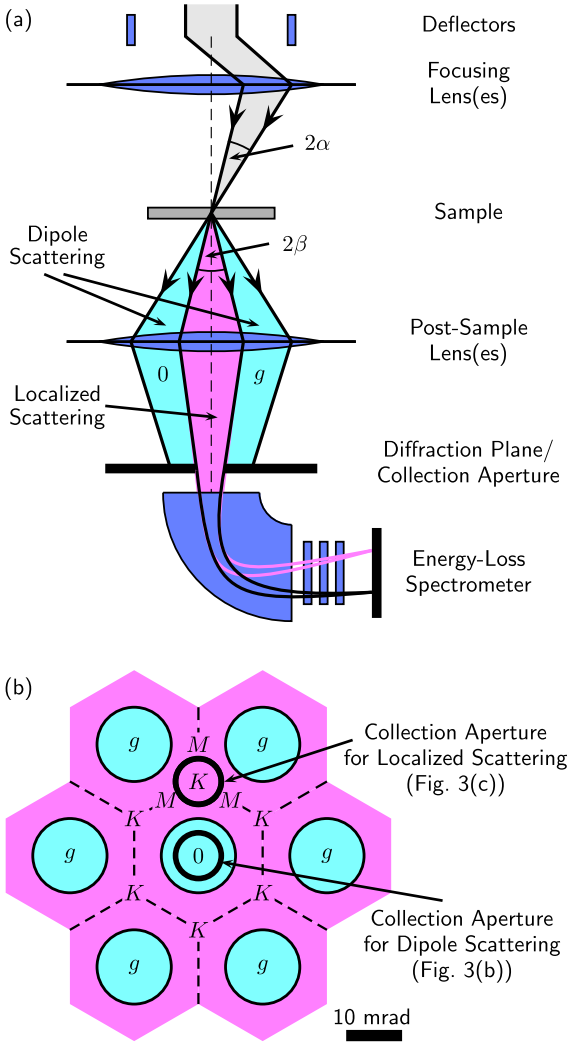

FIG. 2. (a) Electron-beam geometry. Scattering regions labeled 0, g contain elastic and low-angle dipole vibrational scattering (cyan), while regions in between contain higher-angle localized vibrational scattering (magenta). Tilting deflectors control whether localized or dipole scattering enters the energy-loss spectrometer. (b) Diffraction pattern of [0001] h-BN showing collection aperture positions for localized and dipole scattering. The Brillouin zone boundaries are plotted relative to the elastic beam centers.

which type of vibrational scattering is admitted into the spectrometer. Figure 2(b) shows the two collection-aperture positions used in the present experiments on [0001]-oriented BN. We used a convergence semi-angle $\alpha = 6$ mrad, and an EELS collection semi-angle $\beta = 4$ mrad.

Results.—Figure 3(a) shows an ADF image of an [0001] *h*-BN crystal used in our study. The entire crystal comprises an 80 nm-thick platelet, about 2 μm in diameter, suspended over a hole in lacy-carbon film. The ADF image intensity within the BN crystal is largely uniform, indicative of uniform thickness. At the center of the image, the platelet's edge comprises an abrupt change in thickness from zero to 77 ± 2 nm [23]. This thickness change occurs over a transverse distance not more than 2 nm [see the ADF signal in Fig. 3(c)]. The edge acts as a "knife edge" to measure the spatial resolution of vibrational mapping.

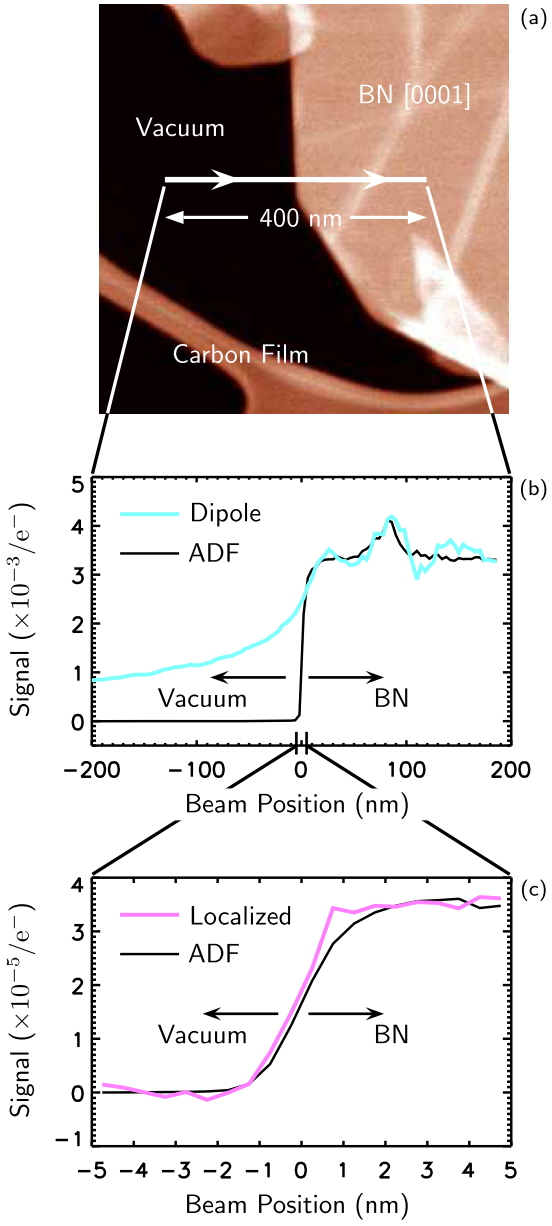

FIG. 3. (a) Annular dark-field (ADF) image of a *h*-BN platelet featuring a sharp edge. (b) Simultaneously acquired dipole-vibrational and ADF signals for beam positions along the path indicated in (a). (c) Simultaneously acquired localized-vibrational and ADF signals for beam positions within ± 5 nm of the edge [note the change in scale compared to (b)]; in (b) and (c) the edge is at approximately 0 nm and the *y*-axis scale indicates the vibrational signal per incident electron.

Figure 3(b) compares the dipole and ADF signals acquired simultaneously as the electron beam traversed the path from the vacuum to BN crystal indicated in Fig. 3(a). The step size was 4 nm and the dwell time was 2 sec/pixel. For the purpose of a direct comparison, the ADF signal intensity has been scaled to match the dipole signal when the beam passes through the crystal. The dipole signal is derived from a spectral peak at 175 meV corresponding to E_{1u} LO modes near the Γ point in Fig. 1. While the ADF signal reveals the sharp edge, the dipole signal, by contrast, is a low-resolution signal that extends hundreds of nanometers into the vacuum [24].

Figure 3(c) shows the simultaneously acquired localized-vibrational and ADF signals within ± 5 nm of the crystal edge [note the dramatically reduced spatial scale compared to Fig. 3(b)]. The step size was 0.5 nm and the total dwell time was 19.6 sec/pixel (accumulated over eight shorter scans). Once again the ADF signal intensity has been scaled for an easy comparison. It is clear that the strength of the vibrational signal follows very closely that of the ADF signal, as must a vibrational signal of the localized type. The vibrational signal increases from a near-constant value of essentially zero in the vacuum to a near-constant maximum value inside the crystal platelet. The variation across the sample edge is well fitted by a complementary error function, for which the associated Gaussian function has a 1.9 nm full-width at half-maximum. Hence the result in Fig. 3(c) constitutes vibrational mapping at a spatial resolution better than 2 nm, which improves on the previous STEM results [1–3] by at least an order of magnitude. In fact, since we expect our beam size to be about 1 nm, the spatial resolution is likely to be limited by the sample edge sharpness, rather than the signal localization or the electron-optical geometry.

The localized vibrational spectra are shown in Fig. 4(a). When the beam passes through the BN crystal, the spectra feature a peak centered at about 160 meV. This peak, owing to its energy loss and the region of the diffraction pattern from which it derives, corresponds to the excitation of TO and LO modes in the vicinity of *K* in Fig. 1. However, since our focused electron beam is a coherent superposition of plane waves, the vibrational excitations involve a coherent superposition of q's: Referring to Fig. 2(b), the superposition involves q vectors that begin anywhere within the "0" beam or, to a lesser extent, one of the "g" beams, and end at a point within the collection aperture. This superposition includes some *M* modes, for example. Referring

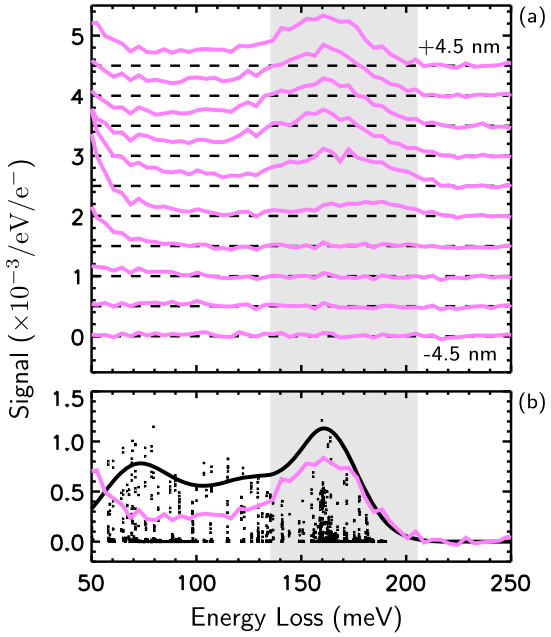

FIG. 4. (a) Localized vibrational spectra for beam positions straddling the specimen edge by ±4.5 nm. Spectra are vertically offset with dashed horizontal lines indicating the zero levels. No background subtraction has been performed. Shaded region indicates the energy window pertaining to the vibrational signal in Fig. 3(c). (b) Comparison of calculated spectrum (black line) and experimental spectrum for beam positioned +4.5 nm inside the BN platelet (magenta line). Points show calculated contributions of individual modes.

back to Fig. 4(a), when the beam passes outside of the sample, the spectra essentially vanish, as should spectra derived from short-ranged scattering. The vibrational signal in Fig. 3(c) is the result of integrating the localized spectra using the 70 meV energy window indicated in Fig. 4(a).

At even lower energy losses, the spectra in Fig. 4(a) also exhibit what appear to be "zero-loss" peaks [the tails of such peaks are visible at the left of Fig. 4(a)]. However, we do not attribute these peaks to vibrational excitations and it appears more likely that they arise from elastic scattering from nonperiodic features of the sample (e.g., defects or amorphous surface layers). This small, but nonzero, elastic intensity *between* the elastic beams also implies that an elastic-plus-dipole double-scattering contribution is present in the spectra of Fig. 4(a). However, our analysis shows that this contribution amounts to, at most, 5% of the spectral signal near 160 meV, which is negligible.

Theory.—Scattering calculations were used to confirm our interpretation of the data in Figs. 3(c) and 4(a). These employ a first-order quantum-mechanical description of the electron-vibrational scattering [6] from the bulk vibrational modes of *h*-BN, using the harmonic and adiabatic approximations. Surface modes were not included since for larger wave vectors they are confined to only a few surface atomic layers. The essence of the calculations is that an excitation of a vibrational mode $q\nu$ (q = wave vector, ν = band index) by a beam-electron wave involves a Møller potential (matrix element) of the form

$$V_{q\nu}(x) = \sum_j x_{q\nu}(j) \cdot \nabla_j \langle V(x) \rangle, \tag{1}$$

where $x_{q\nu}(j)$ is the displacement of the jth ion's nucleus, $\langle V(x) \rangle$ is the thermally averaged Coulomb interaction between the beam electron and the sample, and ∇_j denotes the gradient with respect to the nuclear position of ion j. The Møller potential is the first-order change in $\langle V(x) \rangle$ due to the displacements $x_{q\nu}(j)$. The displacements $x_{q\nu}(j)$ can be written to highlight their wave-vector dependence:

$$x_{q\nu}(j) = \left(\frac{\hbar(\langle n_{q\nu} \rangle + 1)}{2N m_j \omega_{q\nu}} \right)^{1/2} e^*_{q\nu}(j) e^{-iq \cdot x_j}, \tag{2}$$

where $\langle n_{q\nu} \rangle$ is the mode occupancy, m_j the atomic mass, $\omega_{q\nu}$ the vibrational eigenfrequency (cf. Fig. 1), and $e_{q\nu}(j)$ the associated displacement eigenvector.

The calculations also include (multiple) elastic scattering [25], and account for plasmon excitations using Beer's law with a mean-free path of 60 nm [26].

The calculations predict, for our STEM beam passing through BN at the [0001] zone axis, a localized vibrational signal of $4.2 \times 10^{-5}/e^-$, in good agreement with the experimental result of $3.5 \times 10^{-5}/e^-$ obtained in Fig. 3(c). Figure 4(b) shows the calculated spectrum for a spectral resolution corresponding to experiment. The spectrum features a prominent peak at 160 meV, due to optical modes as described above, having a width and strength in good agreement with experiment. The energy-loss axis in Fig. 4 was calibrated with the aid of this peak. The calculations also show a peak at ≈70 meV due to acoustic modes, which is not observed experimentally, possibly due to masking by elastic scattering from nonperiodic features and/or spectrometer aberrations in the experiment. For the current scattering geometry, the calculations predict no significant spectral signal below 50 meV.

Discussion.—The results in Figs. 3 and 4 show that is it possible to use a focused electron beam to map the vibrational excitations of materials at a spatial resolution of the order of one nanometer. This spatial resolution is on par with that achieved in state-of-the-art scanning tunnelling microscope-based tip-enhanced Raman spectroscopy [4]. Here our probe is a finely-controllable electron beam operating in a transmission geometry, which enables analysis of nanomaterials free of thick substrates.

It is significant that our demonstration has used a crystalline material that exhibits strong polarity. Such materials generally possess interesting optical properties at vibrational energies. Our demonstration shows that practical scattering geometries exist which reject the dipole scattering and isolate the weaker localized scattering. Moreover, in the case of conducting materials, our

geometry will also reject scattering from low-energy *electronic* excitations, since they too involve small momentum transfers. An axially aligned beam and an annular EELS collection aperture could be used to further increase the collection efficiency. For example, referring to Fig. 2(b), an annular aperture encompassing (but excluding) the forward-scattered beam, with an annular width of 10 mrad, would improve the collection efficiency more than tenfold.

Summary.—We have demonstrated a spatial resolution of better than 2 nm in vibrational mapping of a crystalline material using a focused monochromated beam of high-energy electrons in an off-axial beam geometry. Our interpretation of experimental results is well supported by our quantum-mechanical calculations of the electron-vibrational scattering. Our results should reconcile the apparently contradictory conclusions of recent theoretical analyses of the spatial resolution achievable in vibrational mapping using high-energy electrons. With further improvements in energy resolution, combining nanometer-scale vibrational analysis with the other high-spatial-resolution signals available in the STEM should provide an extremely powerful toolkit for nanomaterials analysis.

C. D. thanks Jose Menendez for stimulating discussions. Use of facilities in the LeRoy Eyring Center for Solid State Science at Arizona State University is gratefully acknowledged.

*christian.dwyer@asu.edu

[1] O. L. Krivanek, T. C. Lovejoy, N. Dellby, T. Aoki, R. W. Carpenter, P. Rez, E. Soignard, J. Zhu, P. E. Batson, M. Lagos, R. F. Egerton, and P. A. Crozier, Nature (London) **514**, 209 (2014).
[2] T. Miyata, M. Fukuyama, A. Hibara, E. Okunishi, M. Mukai, and T. Mizoguchi, Microscopy **63**, 377 (2014).
[3] P. Rez, T. Aoki, K. March, D. Gur, O. L. Krivanek, N. Dellby, T. C. Lovejoy, S. G. Wolf, and H. Cohen, Nat. Commun. **7**, 10945 (2016).
[4] C. Chen, N. Hayazawa, and S. Kawata, Nat. Commun. **5**, 3312 (2014).
[5] R. Zhang, Y. Zhang, Z. C. Dong, S. Jiang, C. Zhang, L. G. Chen, L. Zhang, Y. Liao, J. Aizpurua, Y. Luo, J. L. Yang, and J. G. Hou, Nature (London) **498**, 82 (2013).
[6] C. Dwyer, Phys. Rev. B **89**, 054103 (2014).
[7] R. F. Egerton, Microsc. Microanal. **20**, 658 (2014).
[8] P. Rez, Microsc. Microanal. **20**, 671 (2014).
[9] A. Howie, Ultramicroscopy **151**, 116 (2015).
[10] N. R. Lugg, B. D. Forbes, S. D. Findlay, and L. J. Allen, Phys. Rev. B **91**, 144108 (2015).
[11] J. R. M. Saavedra and F. J. Garcia de Abajo, Phys. Rev. B **92**, 115449 (2015).
[12] A. Howie, Ultramicroscopy (to be published).
[13] Performed using pseudopotential and local-density approximations [14,15] and the finite-displacement method [16,17].
[14] G. Kresse and J. Furthmüller, Phys. Rev. B **54**, 11169 (1996).
[15] G. Kresse and D. Joubert, Phys. Rev. B **59**, 1758 (1999).
[16] K. Parlinski, Z.-Q. Li, and Y. Kawazoe, Phys. Rev. Lett. **78**, 4063 (1997).
[17] A. Togo, F. Oba, and I. Tanaka, Phys. Rev. B **78**, 134106 (2008).
[18] J. Serrano, A. Bosak, R. Arenal, M. Krisch, K. Watanabe, T. Taniguchi, H. Kanda, A. Rubio, and L. Wirtz, Phys. Rev. Lett. **98**, 095503 (2007).
[19] G. Kern, G. Kresse, and J. Hafner, Phys. Rev. B **59**, 8551 (1999).
[20] K. H. Michel and B. Verberck, Phys. Rev. B **83**, 115328 (2011).
[21] A. A. Govyadinov, A. Konečná, A. Chuvilin, S. Vélez, I. Dolado, A. Y. Nikitin, S. Lopatin, F. Casanova, L. E. Hueso, J. Aizpurua, and R. Hillenbrand, arXiv:1611.05371.
[22] O. L. Krivanek, T. C. Lovejoy, N. Dellby, and R. W. Carpenter, Microscopy **62**, 3 (2013).
[23] Measured by matching experimental and simulated convergent-beam diffraction patterns.
[24] The noisier signal for penetrating beams results from elastic scattering reducing the spectroscopic signal. Our normalization corrects for this reduction, though the noise persists.
[25] The scattering calculations used a "multislice" approach (Ref. [6] and references therein), with a supercell of 16×16 *h*-BN unit cells and 512×512 pixels.
[26] R. F. Egerton, *Electron Energy-Loss Spectroscopy in the Electron Microscope*, 2nd ed. (Plenum Press, New York, 1996).